Local Time Asymmetries in Jupiter's Magnetodisc Currents

C.T.S. Lorch[1], L.C. Ray[1], C.S. Arridge[1], K.K. Khurana[2], C.J. Martin[1], A. Bader[1].

[1]Space & Planetary Physics, Lancaster University, Lancaster, UK
[2]Institute of Geophysics & Planetary Physics, University of California at Los Angeles, Los Angeles, California, USA

Key Points:

- Radial and azimuthal current densities exhibit local time asymmetries throughout the current disk.
- Radial currents flow planetward in noon-dusk sectors and azimuthal currents are weakest through noon.
- Downward field-aligned currents are identified in the noon-dusk magnetosphere.

Corresponding author: Chris Lorch, c.lorch@lancaster.ac.uk

Abstract

We present an investigation into the currents within the Jovian magnetodisc using all available spacecraft magnetometer data up until 28th July, 2018. Using automated data analysis processes as well as the most recent intrinsic field and current disk geometry models, a full local time coverage of the magnetodisc currents using 7382 lobe traversals over 39 years is constructed. Our study demonstrates clear local time asymmetries in both the radial and azimuthal height integrated current densities throughout the current disk. Asymmetries persist within 30 R_J where most models assume axisymmetry. Inward radial currents are found in the previously unmapped dusk and noon sectors. Azimuthal currents are found to be weaker in the dayside magnetosphere than the nightside, in agreement with global magnetohydrodynamic simulations. The divergence of the azimuthal and radial currents indicates that downward field aligned currents exist within the outer dayside magnetosphere. The presence of azimuthal currents is shown to highly influence the location of the field aligned currents which emphasizes the importance of the azimuthal currents in future Magnetosphere-Ionosphere coupling models. Integrating the divergence of the height integrated current densities we find that 1.87 MA R_J^{-2} of return current density required for system closure is absent.

1 Introduction

The existence of a current disk at Jupiter has been well established since the flybys of the Pioneer probes in the 1970s (T. W. Hill & Michel, 1976; Smith et al., 1974). This current disk is a consequence of the strong rotationally driven dynamics that dominate the Jovian magnetosphere. Unlike at Earth where the current sheet is present only in the tail region, Jupiter's current disk is present throughout all local times. A plasma disk is formed from plasma known to originate primarily from the volcanic moon Io, comprising of mostly atomic sulphur and oxygen dissociated from SO_2. Iogenic neutrals are ejected into the local space environment and ionised. Once ionised, Lorentz forces accelerate the plasma towards corotation with the planet, (see review by Khurana et al. (2004); Thomas, Bagenal, Hill, and Wilson (2004)). Radial diffusion of the centrifugally confined plasma via flux-tube interchange events and hot plasma injections produces the plasma disk (T. W. Hill & Michel, 1976; Krupp et al., 2004; Mauk, Williams, McEntire, Khurana, & Roederer, 1999).

The magnetic field geometry of Jupiter's magnetosphere is heavily influenced by the presence of the plasma disk and associated current disk. In order to conserve angular momentum, plasma flowing radially outwards begins to lag corotation. As a consequence the frozen-in field is drawn into a bent back configuration. A $\vec{j}\times\vec{B}$ force, by means of a radial current, is set up to accelerate the plasma back towards corotation (T. Hill, 1979). The flux tube coupling the lagging magnetosphere plasma to the ionosphere will enforce a velocity differential in the ionospheric plasma. Subsequent ion-neutral collisions in the ionosphere exert a frictional torque, balanced by a $\vec{j}\times\vec{B}$ force, transferring angular momentum from the planet to the magnetosphere. It is these corotation enforcement currents which drive the main auroral emission at Jupiter, with the associated electrons precipitating into the planet's atmosphere (Cowley & Bunce, 2001; T. W. Hill, 2001; Khurana et al., 2004; Ray, Ergun, Delamere, & Bagenal, 2010; Southwood & Kivelson, 2001). Radial stretching of the intrinsic field occurs again due to a $\vec{j}\times\vec{B}$ force associated with radial stress balance (Caudal, 1986; Vasyliunas, 1983).

The three dimensional structure of the current disk is complex and time dependent. Arridge, Kane, Sergis, Khurana, and Jackman (2015) provided a review of studies which demonstrated asymmetries in the magnetic field configuration, plasma flow and thickness of the current sheet. The review discussed these complex asymmetries arising due to both internal rotational stresses and external solar wind forcing on the system. The main auroral emission signifies a steady state coupling between the magnetosphere and the ionosphere, hence understanding the asymmetries in the magnetodisc is fundamental to understanding the Magnetosphere-Ionosphere (M-I) coupled system which drives this emission (see review by Ray and Ergun (2012)). Certain features in the main emission are known to be fixed in local time (LT), such as discontinuities in the emission near noon and bright dawn storms (Chané, Palmaerts, & Radioti, 2018; Gustin et al., 2006; Radioti et al., 2008). Ray, Achilleos, Vogt, and Yates (2014) demonstrated such variations in these currents by applying a 1D M-I coupling model at 1 hour LT intervals throughout the Jovian magnetosphere. They showed that the auroral currents were stronger in the dawn sector than the dusk or noon sector by an order of magnitude. The authors emphasized that this approach did not consider azimuthal currents or the azimuthal bendback in the magnetic field, and explicitly called their consideration in future studies.

LT asymmetries have been observed in the UV auroral emissions. Using 1663 FUV Hubble space telescope images Bonfond et al. (2015) showed that 93% of southern and 54% of northern hemispheric images suggested a larger emitted power in the dusk sector than the dawn sector. The southern dusk sector was approximately three times brighter than its dawn counterpart, while northern sectors displayed a relatively similar brightness. The authors attributed this difference to magnetic field variations between hemispheres, arguing also that the southern values are a better representation of the field aligned current (FAC) system associated with the main emission as they lack the superimposed uncertainty of the northern magnetic anomaly.

New insights into the Jovian system are being made with the Juno spacecraft, and in order to incorporate these findings into M-I coupling models the need to move away from symmetric descriptions is apparent. A more complete understanding of the current system and associated magnetic field within the magnetodisc has the potential to alleviate the discrepancies between model predictions and observations. Khurana (2001) determined the radial and azimuthal Height Integrated Current Densities (HICDs) within the magnetodisc using all spacecraft magnetometer data available up until May 31st, 2000 in regions where there was a well defined current sheet. Their findings showed clear LT asymmetries within the system. The divergence of the currents in the magnetodisc indicated the presence of Region 2 currents, Khurana (2001) argued this was due to solar wind forcing on the magnetosphere. From the magnetic field data they were able to quantify the extent of field bend back over LTs, which was included in a later current sheet geometry model (Khurana & Schwarzl, 2005).

Khurana (2001) was limited by the lack of data coverage in the dusk and noon sector of the magnetosphere. Hence the structure of the radial and azimuthal currents in the noon-dusk magnetosphere could not be fully determined. Furthermore, limited insight into the location and strength of return currents was available. As a consequence of this restricted data set simulations have been unable to make comparisons within the dayside magnetosphere Walker and Ogino (2003). Now with updated magnetic field and current sheet geometry models, and by applying automated processes where previous work relied on visual techniques, we build upon this study to provide a full LT coverage of the currents within the Jovian magnetodisc.

In this paper, Section 2 covers the methodology behind extracting the lobe magnetic field values from the magnetometer data, the calculation of the radial and azimuthal HICDs, and how we subsequently deduced the location of the FACs. Our results are displayed in Section 3, and discussion of the results, including their implications for the magnetospheric plasma is undertaken in Section 4. We conclude with a summary of our findings in Section 5.

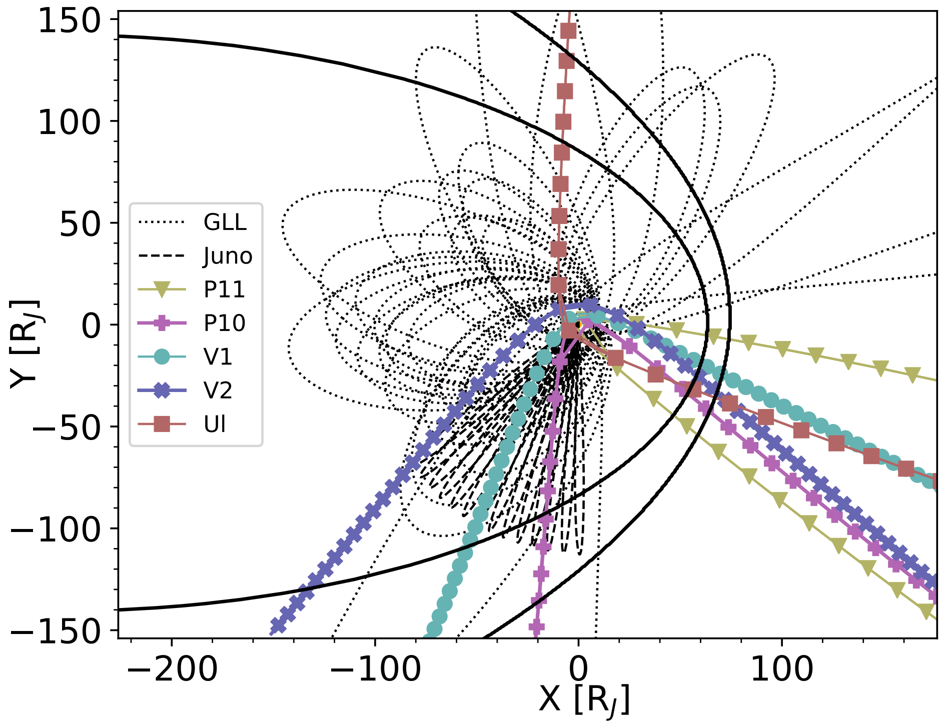

Figure 1. Trajectories of Jovian missions used in this study, projected onto the equatorial plane with the Sun to the right. Also shown are the Joy et al. (2002) bow shock and magnetopause locations for a compressed magnetosphere.

2 Methodology

2.1 Measurements

We utilise magnetometer data from all Jovian missions and flybys, up to and including July 28th 2018. Cassini magnetometer data was not included in this study as the spacecraft did not traverse the current disk. We adopt the same time resolutions as Khurana (2001) for comparison and coherence: 1 minute resolutions were used for Pioneer 10 & 11, Ulysses and Juno, 48 second resolution for Voyager 1 & 2, and 24 second resolution for Galileo Real Time Survey mode. Where finer cadence data was unavailable we used 32 minute averages. To preserve similar temporal resolution between spacecraft 1 minute averaged data was used from Juno. Figure 1 shows an equatorial projection of the spacecraft trajectories to encounter Jupiter. We impose a compressed magnetopause configuration at 62 R_J from Joy et al. (2002) in our analysis. This is illustrated by the solid black lines. Data employed in this study was constrained to regions within the compressed magnetopause with a fixed stand off distance.

2.2 Analysing Magnetometer Data

The observed magnetic field recorded by the spacecraft magnetometers is a summation of an internal dynamo field and an external perturbation field. Hence, to ascertain the magnetic field contribution from the magnetodisc an internal field model must be subtracted from the observed magnetometer data. The JRM09 internal field model

Connerney et al. (2018) is used in this study. JRM09 is a tenth order spherical harmonic expansion of Jupiter's magnetic field with coefficients derived from Juno perijove data (PJ01 through PJ09). Previous models were constructed using data from Pioneer and Voyager flybys, and constrained to the Io auroral footprint (Connerney, Acua, Ness, & Satoh, 1998; Hess, Bonfond, Zarka, & Grodent, 2011), or had an additional dipole superimposed to agree with Hubble space telescope observations (Grodent et al., 2008). The JRM09 model is the ideal candidate for our study as the model exploits low altitude measurements of the magnetic field and so contamination by external fields is negligible. Stallard et al. (2018) gave evidence supporting an immutable intrinsic field between the Galileo era and the Juno era. As most of our data is from this timeframe, we apply JRM09 throughout our study.

Once the internal field is subtracted, the remaining magnetic field is associated with the current disk, magnetopause and tail currents. As we limit our study to distances inside a compressed magnetopause boundary Joy et al. (2002), we neglect contributions from magnetopause currents in our analysis. We assume this is a good approximation as current disk effects dominate in the middle magnetosphere.

It is crucial to work in a current disk reference frame in order to isolate the magnetic perturbation from the current disk. Our new reference frame is a rotating cylindrical reference frame, centered on the planet with ρ pointing radially outward, locally tangential to the current disk surface, z is normal to the current disk, and ϕ completes the right handed system. The angles of rotation are found by determining the normal to a model current disk surface given by Khurana and Schwarzl (2005),

$$Z_{cs} = \sqrt{\left[\left(x_H \tanh\frac{x}{x_H}\right)^2 + y^2\right]} \cdot \tan(\theta_{CS}) \cos(\phi - \phi') + x\left(1 - \tan\left|\frac{x_H}{x}\right|\right) \tan(\theta_{sun}) \quad (1)$$

where x_H is the hinging distance of the current disk, set to be $-47\,R_{\mathrm{J}}$; x and y are the Jupiter-Sun-Orbital positions of the spacecraft, where $\vec{x}$ points towards the sun and $\vec{y}$ points anti-parallel to Jupiter's orbital velocity; θ_{CS} is the tilt angle of the current disk; ϕ is the west longitude of the spacecraft; ϕ' is the prime meridian of the current disk, and θ_{sun} is the angle between the Sun-Jupiter line and the Jovigraphic equator. The model incorporates hinging of the current disk due to solar wind forcing and information delay as a function of radial distance due to wave travel time and field geometry. For further information on this model we refer the reader to Khurana and Schwarzl (2005) and Khurana (1992).

2.3 Calculation of Magnetodisc Currents and their Divergences

Taking Ampere's law in cylindrical coordinates and integrating over the current disk thickness, the radial and azimuthal HICD, J'_ρ and J'_ϕ, may be given as

$$J'_\rho = -\frac{2B_\phi}{\mu_0} \quad (2)$$

$$J'_\phi = \frac{1}{\mu_0}\left(2B_\rho - 2w\frac{\partial B_z}{\partial \rho}\right) \quad (3)$$

where B_ρ, B_ϕ and B_z are the differenced radial, azimuthal and normal field strengths in the lobe regions respectively; w is the half thickness of the current disk, assumed to be 2.5 $\mathrm{R_J}$ to align with other studies (Connerney, 1981; Khurana & Kivelson, 1993). Within the current disk, azimuthal variations in B_z are negligible and hence are not considered in the determination of the radial HICD.

It is important to note that at Jupiter, the lobe region refers to the magnetic field in regions above and below the current disk. Varying the current disk half thickness between 2 $\mathrm{R_J}$ and 10 $\mathrm{R_J}$ does not produce a significant difference in the HICDs outside of 60 $\mathrm{R_J}$. However we find variations in the azimuthal HICD, up to 20% within 50 $\mathrm{R_J}$, and a variance of up to 100% localised at 50 $\mathrm{R_J}$. B_z was determined by fitting a polynomial of the form $B_z(\rho) = \frac{a}{\rho} + \frac{b}{\rho^2} + \frac{c}{\rho^3}$, bounded between $6\,R_\mathrm{J}$ and 100 $\mathrm{R_J}$, to the differenced z component of the magnetic field. Best fits for the coefficients were found to be $a = -1.825 \times 10^2$ $\mathrm{nT\,R_J}$, $b = 1.893 \times 10^4$ $\mathrm{nT\,R_J^2}$ and $c = -8.441 \times 10^4$ $\mathrm{nT\,R_J^3}$.

B_ρ measurements are seen to reverse periodically due to the ~10.3° tilt of the Jovian dipole with respect to the spin axis (Connerney et al., 2018). Periods where spacecraft traversed the lobe region are identified by applying an algorithm that retrieved values at times where the B_ρ component reaches a plateau. Plateaus are defined as regions where consecutive values of B_ρ do not deviate by more than ±7.5% for a period of 30 minutes or more. A variation of ±7.5% is applied as this offers a *juste milieu* by allowing for small fluctuations in the field whilst ignoring the larger variations associated with the traversal of lobes.

This study adopts the modal value of B_ρ, B_ϕ and B_z measured in the determined lobe regions. The mode gives a more accurate value of the lobe field strength, as opposed to the mean which is often skewed by the slowly varying field signatures recorded whilst still within the current disk. Figure 2 demonstrates how the non-lobe field skews the mean, while the modal value lies within a more reasonable estimate of lobe value. For lobes with no mode we adopt the median value. The latter half of the Ulysses flyby and intervals from the Juno dataset were excluded due to their large deviations from the equatorial plane. Data outside of the fixed magnetopause boundary was also excluded. In total 7382 valid intervals were retrieved, we believe this number to be biased. For example a sharp fluctuations in the lobe field will result in two readings being returned, one prior to, and one after the fluctuation. Both of these recordings are returned and used in this study. Hence the number of true lobes recorded will be less than what were retrieved.

3 Results

3.1 Height Integrated Current Density

The radial and azimuthal HICDs were calculated using the modal values for B_ρ, B_ϕ and B_z in the lobe regions. We illustrate this in Figure 3, which shows the radial HICD (3a), the azimuthal HICD (3c) and their binned averages (3b and 3d, respectively). For the radial HICDs warmer colours indicate outward radial currents, while cooler colours indicate planetward radial currents. The azimuthal currents all flow in the direction of corotation and are shown using a natural log scale.

Initially, we see a clear asymmetry in the averaged radial currents. Strong outward radial currents dominate the midnight through dawn magnetosphere, while weaker inward currents exist from noon through dusk region. Within 40 $\mathrm{R_J}$ strong outward radial currents are present, but weaken at noon. Within distances of 20 $\mathrm{R_J}$, radial currents appear to be weaker in the post dusk sector than at other LTs. The azimuthal HICDs, shown in figures 3c and 3d, decay with radial distance. The azimuthal HICDs are larger in the midnight through dawn sectors than in noon through dusk.

These asymmetries are better seen in Figure 4, which shows the variation in the HICDs over local time at fixed radial distances. Here, data is binned in 5 $\mathrm{R_J}\times$ 3hr bins, centred at 5 $\mathrm{R_J}$ intervals. In both the radial and azimuthal HICDs we see local time asymmetries begin to develop with radial distance from 15 $\mathrm{R_J}$. For the radial currents, a maxima develops around 6LT with a minima at noon. This minima shifts to around 18UT at larger radial distances. The azimuthal currents exhibit a noon-midnight asymmetry. Azimuthal currents are weakest in the around noon, and largest at midnight. The az-

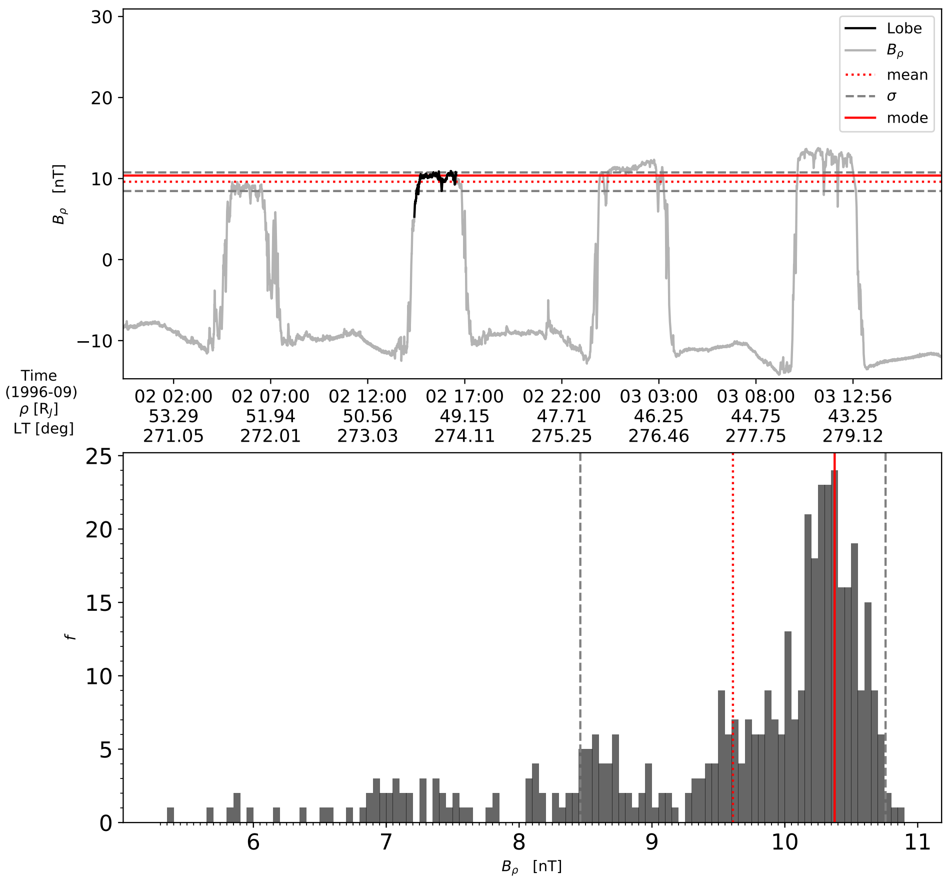

Figure 2. *(Top)* The radial component of the differenced field can be seen in grey. The dark region indicates a single lobe region determined by the algorithm. The algorithm returns consecutive magnetic field measurements with less than a 7.5% for a period of more than 30 minutes. *(Bottom)* A frequency histogram of the magnetic field strength during the lobe traversal, shown as a thick black line in the top panel. In both panels dashed grey lines indicate the standard deviation of the lobe values, the solid red line indicates the modal value and the dashed red line indicates the mean.

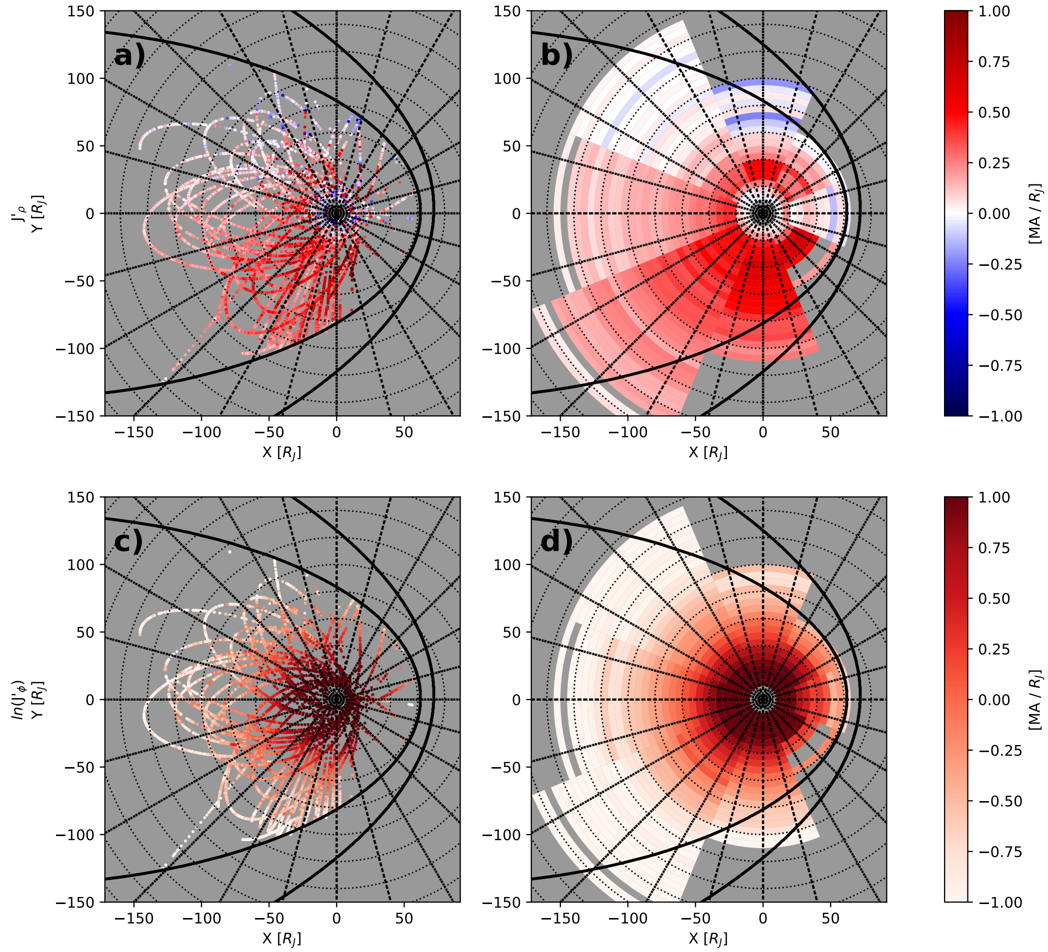

Figure 3. HICD from lobe regions determined by algorithm. (a) The height integrated radial current density. Warmer (cooler) colours indicate outward (inward) flowing radial currents. These values are binned and averaged in (b). (c) The height integrated azimuthal current density. Note the log scale on the colour axis. Current flow is in the direction of corotation and again the values are binned and averaged in (d). Concentric dotted rings are placed at intervals of 20 R_J. 1 hour LT divisions are separated by straight dotted lines. Solid black lines represent the magnetopause and bow shock boundaries from Joy et al. (2002).

imuthal currents fall off rapidly with increasing distance, becoming comparable to the radial currents further from the planet.

In order to highlight the variation in radial and azimuthal currents with local time, we bin our results in 6hr LT regions, centred on midnight, dawn, dusk, and noon. This is shown in Figures 5 and 6 for the radial and azimuthal HICDs, respectively. Black dots represent the HICD calculated from lobe values and the red line represents the mean binned every 5 R_J. Radial currents are seen to peak around 30 R_J then steadily decrease. The azimuthal currents decrease in a $1/\rho$ fashion. For both the radial and azimuthal components, currents in the noon sector are weaker than the other sectors.

The errors in Figures 4, 5 and 6 are given by the standard error of the mean, ϵ, calculated as: $\epsilon = \frac{\sigma}{\sqrt{n}}$, where σ is the standard deviation of the averaged data, and n is the number of data points within the bin. The mean was chosen over the median to represent our results as the associated error was considerably less than the median absolute error obtained from the median average.

3.2 Divergence of the Height Integrated Current Density

Figure 7 shows the divergence of the radial (7a), azimuthal (7b) and perpendicular (7c) HICD. From current continuity:

$$\nabla \cdot J' = \nabla_{\perp} \cdot J'_{\perp} + \nabla_{||} \cdot J'_{||} = 0 \tag{4}$$

Hence we relate the divergence of our radial and azimuthal components, $\nabla J'_{\rho}$ and $\nabla J'_{\phi}$ to the divergence of the parallel currents. Warmer (cooler) colours indicate current being added to (removed from) the denoted component. Radial currents are enhanced within the inner middle magnetosphere, whilst depleted through noon and dusk. Azimuthal currents are fed in the dusk magnetosphere, and removed at dawn, consistent with the analysis of Khurana (2001).

From current continuity, the perpendicular and parallel divergence must equal 0. Therefore, the sum of the radial and azimuthal current divergence can be used to reveal the location of upward and downward FACs, where again warmer (cooler) colours indicate upward (downward) FACs. Our deduced FAC locations agree with those from Khurana (2001), however there is now complete coverage in the dusk and noon sector due to the additional data.

4 Discussion

We identify 7382 traversals using data spanning nearly 5 decades. Over this time, the solar wind conditions at Jupiter would have varied widely. Though the orientation of the interplanetary magnetic field has little effect on asymmetries in the system, the dynamic pressure of the solar wind does (Cowley & Bunce, 2001). For example, a compression of the magnetosphere due to an increase in solar wind dynamic pressure forces plasma radially inward. This increases its angular velocity and consequently decreases the corotation enforcement currents, altering the magnetic field geometry. By binning and averaging over all data available we do not consider temporal fluctuations, such as those associated with variations in the solar wind dynamic pressure or perturbations in the current disk. Therefore, this analysis presents an average view of Jupiter's current disk where the variance in the data, captured in our error analysis, reflects some of these natural fluctuations.

The radial currents in Figures 3a and 3b are associated with corotation enforcement. Outward radial currents act to accelerate plasma towards corotation, whilst inward radial currents decelerate the plasma. Peaks occurring around 30 R_J in Figure 5 are consistent with the location of corotation breakdown inferred from auroral observations and numerous models Clarke et al. (2004); Nichols and Cowley (2004); Ray et al. (2010); Ray, Ergun, Delamere, and Bagenal (2012). Azimuthal currents in Figure 6c and 6d are associated with the $\vec{j} \times \vec{B}$ forces acting to balance radial stresses. The presence of weaker radial and azimuthal currents at noon is in part due to the influence of solar wind on the Jovian magnetosphere. As plasma rotates through dawn into the dayside magnetosphere, it is constrained by the magnetopause and forced closer to the planet. As a consequence its velocity increases and $\vec{j} \times \vec{B}$ force required to keep the plasma in corotation is decreased (Chané, Saur, Keppens, & Poedts, 2017; Kivelson & Southwood, 2005; Walker & Ogino, 2003). Additionally, the solar wind dynamic pressure acts to balance the outward radial stresses and so weaker azimuthal currents are present in the dayside magnetosphere.

Asymmetries are prevalent throughout the magnetosphere, demonstrating the the influence of the solar wind on the Jovian system. While these are strongest in the middle-

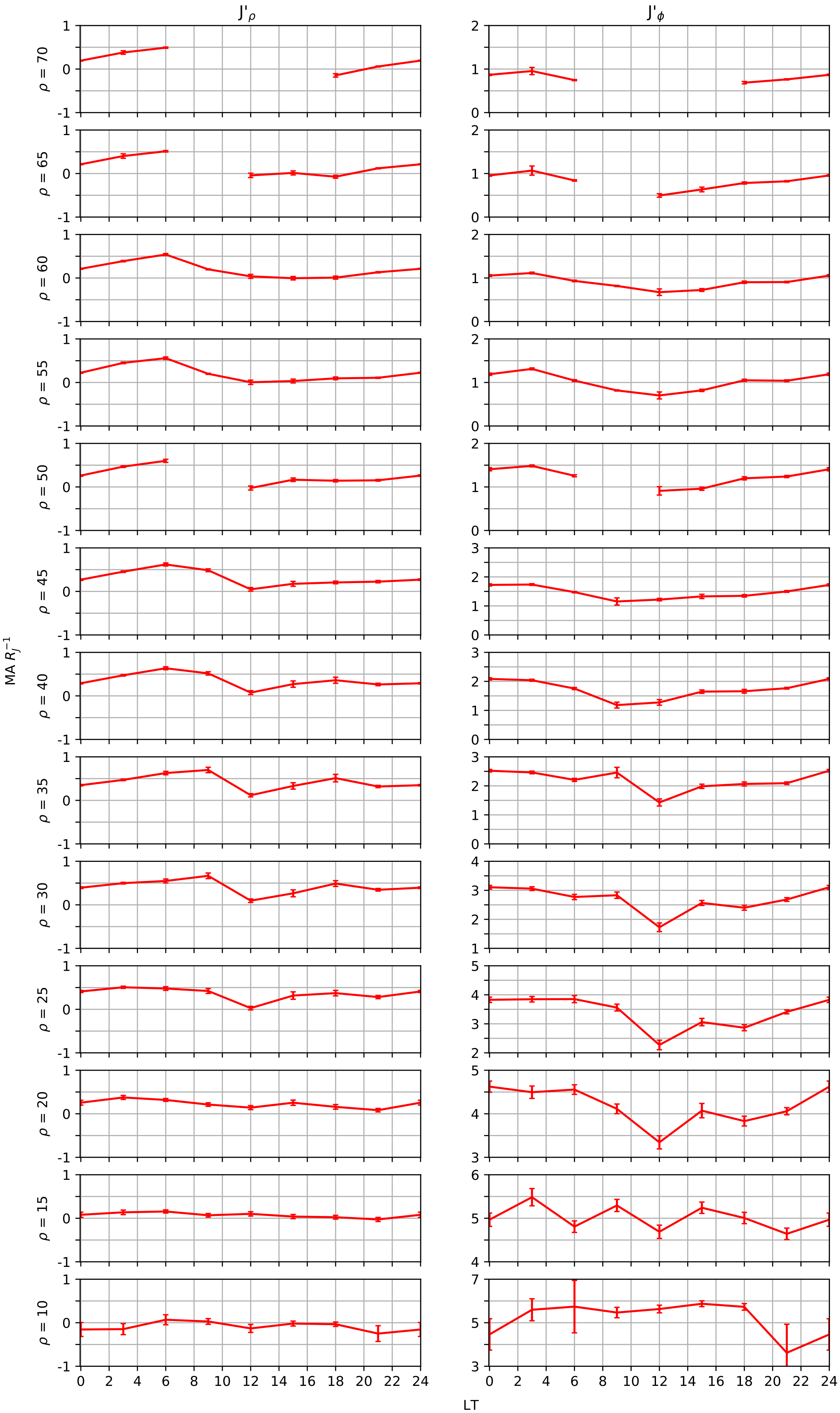

Figure 4. The mean radial *(left)* and azimuthal *(right)* HICD over all LTs, averaged in radial bins of 5 R_J. Results are averaged into each sector. Error bars represent the standard error of the mean.

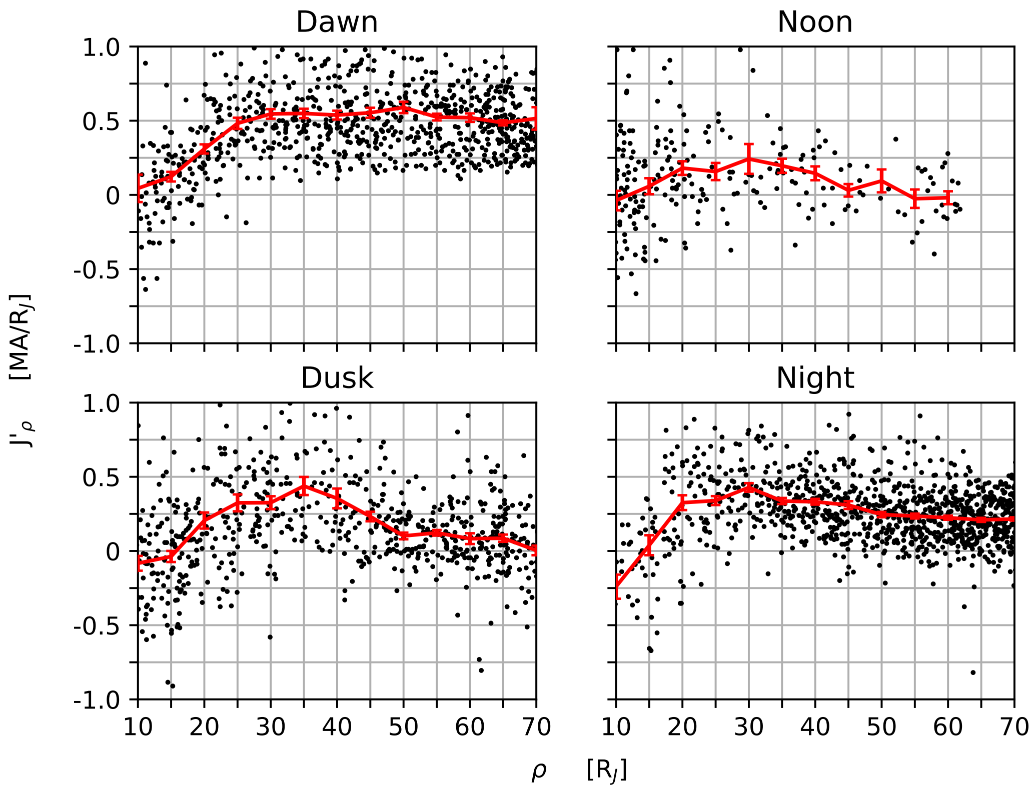

Figure 5. The radial HICD shown against radial distance from the planet binned in LT sectors. HICDs from lobe traversals are represented by black dots. The red line is the mean of the $5\,R_{\mathrm{J}}$ bins. Error bars represent the standard error of the mean.

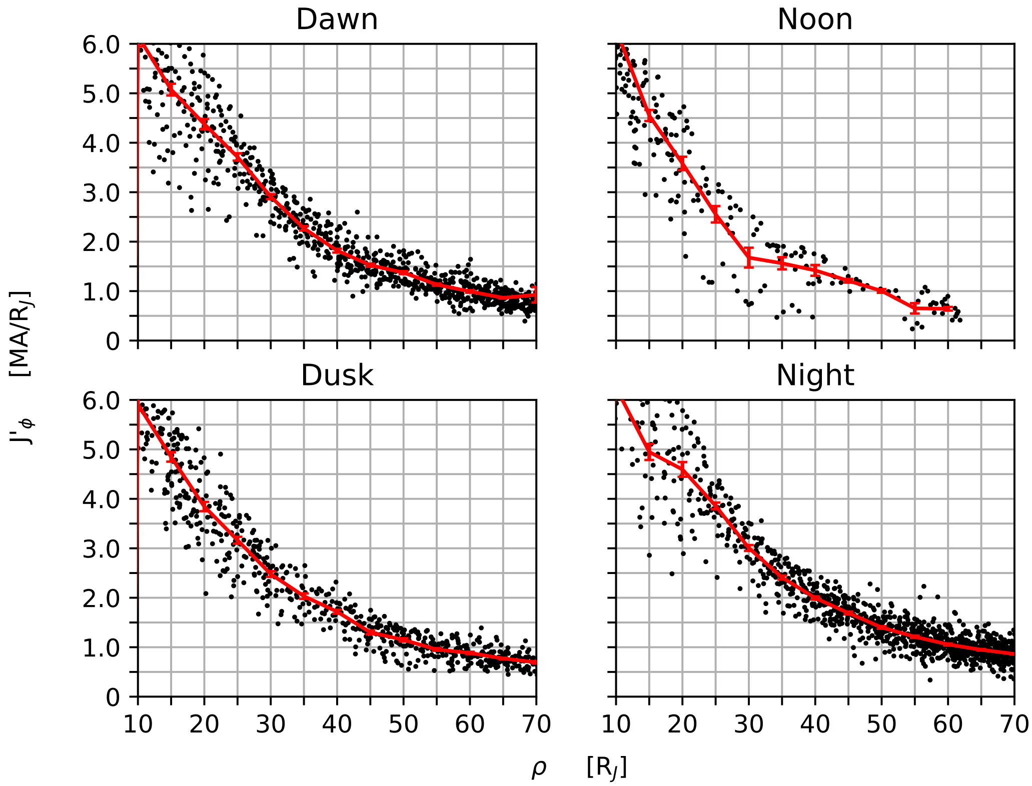

Figure 6. The azimuthal HICD shown against radial distance from the planet binned in LT sectors. HICDs from lobe traversals are represented as black dots. The red line is the mean of the $5\,R_\mathrm{J}$ bins. Error bars represent the standard error of the mean.

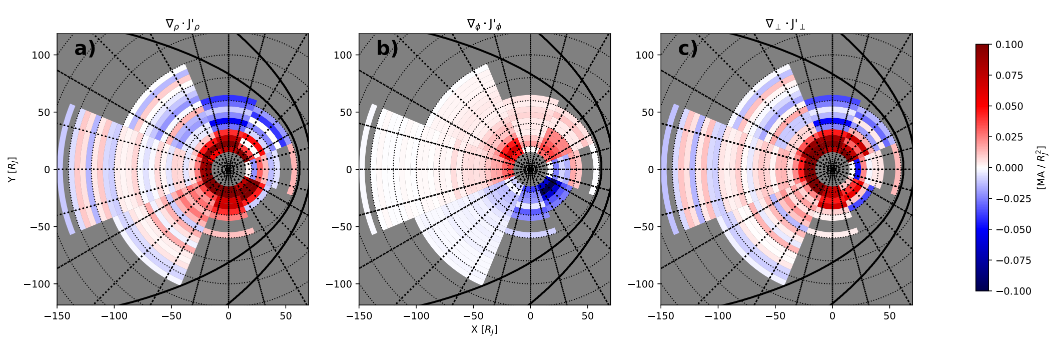

Figure 7. The divergence of the HICD for the (a) radial (b) azimuthal and (c) perpendicular components, in a similar format to Figure 3. The divergence of the perpendicular components is analogous to the parallel current density.

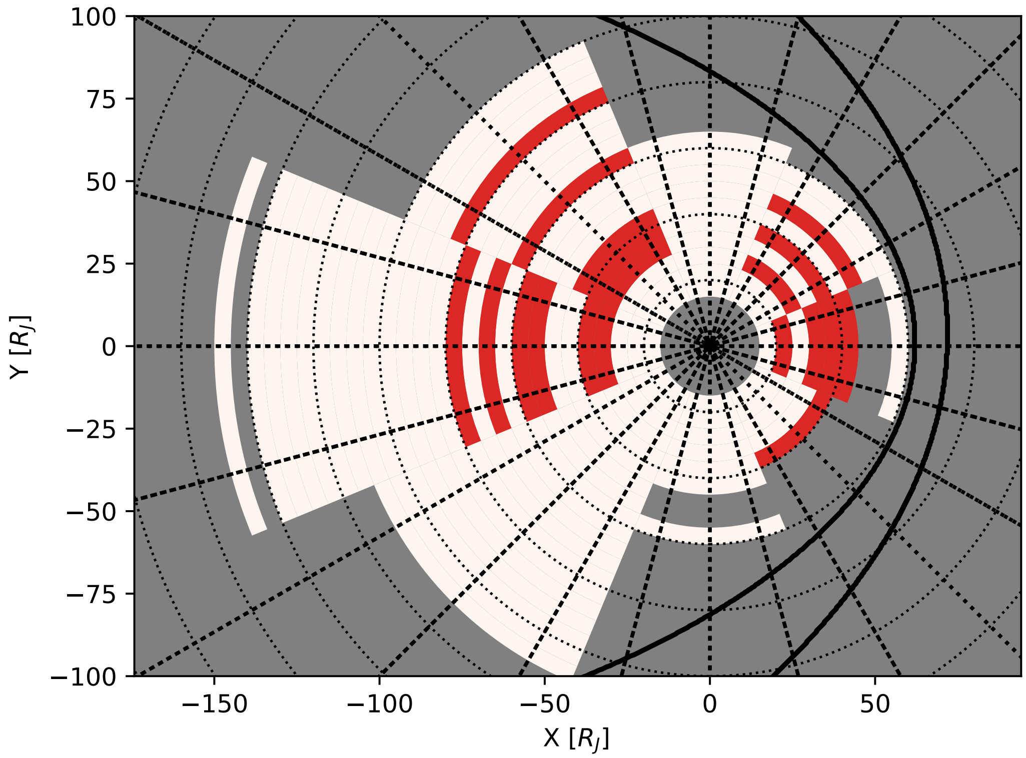

Figure 8. A comparison of the radial and azimuthal divergences. Red regions denote where $\nabla_\phi \cdot J'_\phi > \nabla_\rho \cdot J'_\rho$, white regions denote where $\nabla_\rho \cdot J'_\rho > \nabla_\phi \cdot J'_\phi$. (In similar format to Figure 3)

to-outer magnetosphere, the inner magnetosphere is also affected. At 20 R_J, the nightside radial and azimuthal currents exceed the dayside by $\sim$30% as shown in Figures 5 and 6. The asymmetries increase with radial distance. Outside 40 R_J the dawn-dusk asymmetry in the HICD is stark. Strong outward currents in the dawn sector transition into inward currents through noon into the dusk sector. These currents act to accelerate plasma through dawn into the dayside magnetosphere and decelerate it through the noon to post-dusk sector. Radial currents in the dawn sector have little variation with radial distance, but decrease steadily in the other three LT sectors, with the noon and dusk currents falling off more rapidly than the night sector. It should be noted that around 50 R_J the currents are highly dependent on the choice of current disk thickness, and so our results may vary by $\pm$100%.

The development of LT asymmetries is highlighted in Figure 4. Transitioning from smaller to larger radial distances, we see a fairly uniform radial HICD, growing increasingly with respect to ρ. The weakest radial currents are observed between 12:00 - 18:00, agreeing with findings by Ray et al. (2014), who showed a region of weaker current density in the post noon sector. Azimuthal currents are seen to fall off with distance. As in Khurana (2001), a peak begins to develop in the radial and azimuthal HICD around 06:00LT and 00:00LT respectively, but now we see the weakest currents are present at noon. A similar development has also been reported at Saturn by Martin and Arridge (2019) where a minimum occurs in the HICD through the noon-dusk sector.

The asymmetries determined in the HICDs are consistent with those observed in other datasets. Variations in the plasma flow velocity have been observed in Galileo energetic particle data by Krupp et al. (2001). They showed pronounced LT asymmetry in plasma velocities within 50 R_J, with dawn-noon velocities being greater than noon-dusk velocities. However, plasma data is limited outside 50 R_J in the dusk sector. Within the inner-to-middle magnetosphere, plasma flows derived by Bagenal, Wilson, Siler, Paterson, and Kurth (2016) were slightly larger in the dawn sector than the dusk sector, however their study only extended to 30 R_J. Results by Bunce and Cowley (2001a) showed that the current disk field falls off more rapidly in the dayside than at similar distances in the nightside.

Walker and Ogino (2003) applied a global magnetohydrodynamic (MHD) model to investigate the influence of the solar wind on the structure of currents within the Jovian magnetosphere. In their study they compared their simulated currents with the findings of Khurana (2001), however a system-wide comparison could not be made as a result of limited Galileo orbiter data. Our study has now revealed the structure of currents within these regions. Though the simulated current densities are overall much weaker than our observed HICDs, the asymmetries present in the simulation are in qualitative agreement with these observations. Outward radial currents are predicted in the pre-noon sector, and inward radial currents in the post-noon sector. This is consistent with the observations of a transition from outward to inward radial currents within the noon magnetosphere. However the inward radial currents predicted in the midnight sector are not present in this study. Similarly, using a 3D global MHD simulation, Chané et al. (2018) investigated the cause of localised peaks in auroral emissions. They showed flux tubes being accelerated through dawn into noon before decelerating and moving in towards the planet. The presence of strong outward radial currents within the dawn sector in our results agree with the results from this simulation.

Examining the divergences of the perpendicular currents, Figure 7a illustrates positive radial divergences present throughout all LTs within 30 R_J and up to 70 R_J in the dawn sector suggesting an increasing radial current, whilst current is being removed within the post-noon to dusk side magnetosphere. For the azimuthal component in 7b, we find the same dawn-dusk asymmetry reported by Khurana (2001), indicating an azimuthal current loss in the dawn magnetosphere and a gain in the dusk sector. A strong downward current region can be seen in the dayside magnetosphere. It is possible that this could be related to the auroral discontinuity observed by Radioti et al. (2008), however we have not mapped the signature to confirm this. Radial HICDs play a key role in determining the location of the FACs. As can be seen in Figure 7, the divergence of perpendicular currents are largely similar to the divergence of radial currents, with some variation in the inner regions due to a strong azimuthal divergence in the currents. This highlights the importance of considering both radial and azimuthal currents when describing the MI coupling system responsible for Jupiter's auroral emissions.

A prominent feature in the tail region is an alternation between positive and negative divergences in the radial component, and subsequently the perpendicular current divergence. This affect, referred to as "striping" by Martin and Arridge (2019), is an artifact of the differencing method. Small variations between adjacent bins, containing low counts, result in the appearance of a larger divergence. This feature is more pronounced in the radial divergence due to the smaller magnitude values. We find this affect can be mitigated by increasing the bin size to encompass more data points with the drawback of decreased resolution, or by bootstrapping data within the bins. Our bin choice produced an agreeable trade off between the conservation of fine structures and minimizing the striping effect.

Figure 8 presents a comparison of the radial and azimuthal divergences. Regions where the divergence of the azimuthal (radial) currents are greater than the radial (azimuthal) currents are coloured red (white). In white regions the divergence of perpendicular currents is determined largely by the radial currents. In all LT sectors, with the exception of the pre dawn sector, the divergence of the azimuthal currents influences the presence of FACs to a similar degree as the divergence of the radial currents. When utilizing M-I coupling models to describe the Jovian current system, it is therefore important to consider not only the effect on FACs by the azimuthal currents, but also the effect of LT asymmetries in determining their location and magnitude. Prevailing discrepancies between 1D M-I coupling models and observations could be a consequence of neglecting the effects of azimuthal currents in the Jovian system. Future M-I coupling models should strive to amalgamate both the influence of radial and azimuthal currents in order to obtain a more realistic description of the system. This could be done through an empirical description of the HICDs, however we leave this for future work. At Saturn, the divergence of radial currents is much smaller in magnitude than the divergence of azimuthal currents. As such, the divergence of azimuthal currents largely determines the location of the FACs at Saturn Martin and Arridge (2019) and should be strongly considered.

We note that upward FACs dominate the inner (40 R_J) region of the magnetodisc, however there are much stronger positive divergences between 16:30LT and 01:30LT, and weaker, sometimes negative divergences at approximately 07:30LT – 13:30LT. Radioti et al. (2008) suggested that these return currents within the dayside magnetosphere would correspond to discontinuities observed in the main auroral emission. The strong upward FACs found in the dawn sector could be attributed to the shearing motion of flux tubes described by the Chané et al. (2018) simulation. As this is a common feature, we would expect it to appear in our time averaged results and would act to enhance FACs in the region. Again predictions made by Walker and Ogino (2003) are consistent with our findings. In the Khurana (2001) study, return FACs were not identified in the dusk-noon region due to the lack of available magnetometer data. With the increased coverage used in this study we are able to reveal evidence of current closure in outer dusk-noon magnetosphere, radially adjacent to regions of strong upward FACs.

By summing over the divergence of the perpendicular currents throughout the system, an overall positive divergence of 1.87 MA R_J^{-2} is calculated. As current continuity must be maintained, the missing return currents must exist in the unmapped regions of the system i.e. dayside and magnetopause regions. This value assumes that the effect of magnetopause currents is negligible in the current disk. As mentioned previously, by working within the boundary of a compressed magnetosphere, we begin to limit the influence of these currents on our results. Furthermore, the magnetopause currents are external to the currentdisk region and take the form of a Laplacian field inside the magnetosphere. For a Laplacian field the two terms of Eq 3. exactly cancel, providing no contribution to the local azimuthal currents. Variations in the current disk thickness would influence the strength of the azimuthal currents and alter this value. This demonstrates the need for a description of the spatial variation of current disk thickness which could help to provide a more accurate representation of the azimuthal currents within 50 R_J. This would further constrain the contribution of azimuthal currents to the location and magnitude of FACs.

5 Summary

We have presented an analysis of the current structure within the Jovian magnetodisc using all magnetometer data available until 28th July 2018. We build upon previous work by Khurana (2001) using the latest internal field model, current disk geometry model, and an automated lobe finding process. In doing so we are able to provide a high resolution, full LT coverage of the radial and azimuthal HICDs in the Jovian current disk. Our conclusions are as follows:

1. Asymmetries in both radial and azimuthal HICDs exist within the inner portion of the middle magnetosphere, some manifesting within 20 R_J.
2. Both radial and azimuthal currents are weakest in the dayside magnetosphere.
3. Azimuthal currents are shown to play a key role in determining the location of FACs.
4. By summing over all known perpendicular divergences a net positive divergence of 1.87 MA R_J^{-2} is found. We postulate this to be balanced along the magnetopause and/or in the tail region.

We therefore suggest that future M-I coupling models should take into account not only the presence of radial currents but also azimuthal currents, and the asymmetries found in both. Furthermore, when utilizing and constructing models of the current disk, it is paramount that the asymmetries be taken into consideration. Future work aims to produce an empirical description of these asymmetries, such that they can be readily integrated into M-I coupling models, as well as producing a full spatial description of the variation in current disk thickness.

Acknowledgments

The authors thank the reviewers for their highly constructive and detailed feedback. C.T.S.L was funded by an STFC Studentship. L.C.R was funded by STFC Consolidated Grant ST/R000816/1 to Lancaster University. C.S.A was funded by a Royal Society Research Fellowship and Consolidated Grant ST/R000816/1. C.J.M was funded by a Lancaster University FST Studentship and Consolidated Grant ST/R000816/1. A.B was funded by a Lancaster University FST Studentship. Collaborations with K.K.K were made possible thanks to support from the Royal Astronomical Society travel grant. Magnetometer data used in this work was retrieved from the Planetary Data System database (https://pds-ppi.igpp.ucla.edu/).

References

Arridge, C. S., Kane, M., Sergis, N., Khurana, K. K., & Jackman, C. M. (2015). Sources of Local Time Asymmetries in Magnetodiscs. *Space Science Reviews*, *187*(1), 301–333. doi: 10.1007/s11214-015-0145-z

Bagenal, F., Wilson, R. J., Siler, S., Paterson, W. R., & Kurth, W. S. (2016).

Survey of Galileo plasma observations in Jupiter's plasma sheet: Galileo Plasma Observations. *Journal of Geophysical Research: Planets*, *121*(5), 871-894. Retrieved from `http://doi.wiley.com/10.1002/2016JE005009` doi: 10.1002/2016JE005009

Bonfond, B., Gustin, J., Grard, J.-C., Grodent, D., Radioti, A., Palmaerts, B., ... Tao, C. (2015). The far-ultraviolet main auroral emission at Jupiter – Part 1: Dawndusk brightness asymmetries. *Annales Geophysicae*, *33*(10), 1203–1209. Retrieved 2019-02-22, from `https://www.ann-geophys.net/33/1203/2015/` doi: 10.5194/angeo-33-1203-2015

Bunce, E. J., & Cowley, S. W. H. (2001a). Divergence of the equatorial current in the dawn sector of Jupiters magnetosphere: analysis of Pioneer and Voyager magnetic field data. *Planetary and Space Science*, *49*, 25.

Caudal, G. (1986). A self-consistent model of Jupiter's magnetodisc including the effects of centrifugal force and pressure. *Journal of Geophysical Research*, *91*. Retrieved from `http://doi.org/10.1029/JA091iA04p04201` doi: 10.1029/JA091iA04p04201

Chané, E., Palmaerts, B., & Radioti, A. (2018). Periodic shearing motions in the Jovian magnetosphere causing a localized peak in the main auroral emission close to noon. *Planetary and Space Science*, *158*, 110–117. Retrieved from `https://linkinghub.elsevier.com/retrieve/pii/S0032063317304737` doi: 10.1016/j.pss.2018.04.023

Chané, E., Saur, J., Keppens, R., & Poedts, S. (2017). How is the Jovian main auroral emission affected by the solar wind? *Journal of Geophysical Research: Space Physics*. Retrieved from `http://doi.wiley.com/10.1002/2016JA023318` doi: 10.1002/2016JA023318

Clarke, J., Grodent, D., Cowley, S., Bunce, E., Zarka, P., Connerney, J., & Satoh, T. (2004). Jupiter's Aurora. In F. Bagenal, T. Dowling, & W. McKinnon (Eds.), *Jupiter the planet, satellites and magnetosphere* (p. 639 - 670). Cambridge: Cambridge University Press.

Connerney, J. E. P. (1981). The magnetic field of Jupiter: A generalized inverse approach. *Journal of Geophysical Research: Space Physics*, *86*, 7679–7693. Retrieved 2018-10-12, from `http://doi.wiley.com/10.1029/JA086iA09p07679` doi: 10.1029/JA086iA09p07679

Connerney, J. E. P., Acua, M. H., Ness, N. F., & Satoh, T. (1998). New models of Jupiter's magnetic field constrained by the Io flux tube footprint. *J. of Geophys. Res.: Space Physics*, *103*, 11929–11939. doi: 10.1029/97JA03726

Connerney, J. E. P., Kotsiaros, S., Oliversen, R. J., Espley, J. R., Joergensen, J. L., Joergensen, P. S., ... Levin, S. M. (2018). A New Model of Jupiter's Magnetic Field From Juno's First Nine Orbits. *Geophysical Research Letters*, *45*(6), 2590–2596. doi: 10.1002/2018GL077312

Cowley, S., & Bunce, E. (2001). Origin of the main auroral oval in Jupiter's coupled magnetosphereionosphere system. *Planetary and Space Science*, *49*(10), 1067–1088. doi: 10.1016/S0032-0633(00)00167-7

Grodent, D., Bonfond, B., Grard, J.-C., Radioti, A., Gustin, J., Clarke, J. T., ... Connerney, J. E. P. (2008). Auroral evidence of a localized magnetic anomaly in Jupiter's northern hemisphere. *J. of Geophys. Res.: Space Physics*, *113*, n/a–n/a. doi: 10.1029/2008JA013185

Gustin, J., Cowley, S. W. H., Grard, J.-C., Gladstone, G. R., Grodent, D., & Clarke, J. T. (2006). Characteristics of Jovian morning bright FUV aurora from Hubble Space Telescope/Space Telescope Imaging Spectrograph imaging and spectral observations. *Journal of Geophysical Research*, *111*. Retrieved 2019-03-11, from `http://doi.wiley.com/10.1029/2006JA011730` doi: 10.1029/2006JA011730

Hess, S. L. G., Bonfond, B., Zarka, P., & Grodent, D. (2011). Model of the Jovian magnetic field topology constrained by the Io auroral emissions. *J. of Geophys.*

Res.: Space Physics, *116*. Retrieved 2018-10-12, from http://doi.wiley.com/10.1029/2010JA016262 doi: 10.1029/2010JA016262

Hill, T. (1979). Inertial limit on corotation. *J. of Geophys. Res.*, *84*, 6554. doi: 10.1029/JA084iA11p06554

Hill, T. W. (2001). The Jovian auroral oval. *J. of Geophys. Res.: Space Physics*, *106*, 8101–8107. doi: 10.1029/2000JA000302

Hill, T. W., & Michel, F. C. (1976). Heavy ions from the Galilean satellites and the centrifugal distortion of the Jovian magnetosphere. *Journal of Geophysical Research*, *81*(25). Retrieved from http://doi.wiley.com/10.1029/JA081i025p04561 doi: 10.1029/JA081i025p04561

Joy, S. P., Kivelson, M. G., Walker, R. J., Khurana, K. K., Russell, C. T., & Ogino, T. (2002). Probabilistic models of the Jovian magnetopause and bow shock locations. *J. of Geophys. Res.*, *107*. doi: 10.1029/2001JA009146

Khurana, K. K. (1992). A generalized hinged-magnetodisc model of Jupiter's nightside current sheet. *J. of Geophys. Res.*, *97*, 6269. doi: 10.1029/92JA00169

Khurana, K. K. (2001). Influence of solar wind on Jupiter's magnetosphere deduced from currents in the equatorial plane. *J. of Geophys. Res.: Space Physics*, *106*, 25999–26016. doi: 10.1029/2000JA000352

Khurana, K. K., & Kivelson, M. G. (1993). Inference of the angular velocity of plasma in the Jovian magnetosphere from the sweepback of magnetic field. *Journal of Geophysical Research: Space Physics*, *98*, 67–79. Retrieved 2018-11-15, from http://doi.wiley.com/10.1029/92JA01890 doi: 10.1029/92JA01890

Khurana, K. K., Kivelson, M. G., Vasyliunas, V. M., Krupp, N., Woch, J., Lagg, A., ... Kurth, W. S. (2004). The Configuration of Jupiter's Magnetosphere. In F. Bagenal, T. Dowling, & W. McKinnon (Eds.), *Jupiter the planet, satellites and magnetosphere* (p. 593 - 616). Cambridge: Cambridge University Press.

Khurana, K. K., & Schwarzl, H. K. (2005). Global structure of Jupiter's magnetospheric current sheet. *J of Geophys. Res.*, *110*. doi: 10.1029/2004JA010757

Kivelson, M. G., & Southwood, D. J. (2005). Dynamical consequences of two modes of centrifugal instability in Jupiter's outer magnetosphere. *Journal of Geophysical Research*, *110*. Retrieved from http://doi.wiley.com/10.1029/2005JA011176 doi: 10.1029/2005JA011176

Krupp, N., Lagg, A., Livi, S., Wilken, B., Woch, J., Roelof, E. C., & Williams, D. J. (2001). Global flows of energetic ions in Jupiter's equatorial plane: First-order approximation. *J. of Geophys. Res.: Space Physics*, *106*, 26017–26032. doi: 10.1029/2000JA900138

Krupp, N., Vasyliunas, V., Woch, J., A, L., Khurana, K., Kivelson, M., ... Paterson, W. (2004). Dynamics of the Jovian Magnetosphere. In F. Bagenal, T. Dowling, & W. McKinnon (Eds.), *Jupiter the planet, satellites and magnetosphere* (p. 617 - 638). Cambridge: Cambridge University Press.

Martin, C. J., & Arridge, C. S. (2019). Current Density in Saturn's Equatorial Current Sheet: Cassini Magnetometer Observations. *Journal of Geophysical Research: Space Physics*, *124*(1), 279-292. Retrieved from http://doi.wiley.com/10.1029/2018JA025970 doi: 10.1029/2018JA025970

Mauk, B. H., Williams, D. J., McEntire, R. W., Khurana, K. K., & Roederer, J. G. (1999). Storm-like dynamics of Jupiter's inner and middle magnetosphere. *Journal of Geophysical Research: Space Physics*, *104*. Retrieved from http://doi.wiley.com/10.1029/1999JA900097 doi: 10.1029/1999JA900097

Nichols, J. D., & Cowley, S. W. H. (2004). Magnetosphere-ionosphere coupling currents in Jupiter's middle magnetosphere: effect of precipitation-induced enhancement of the ionospheric Pedersen conductivity. *Annales Geophysicae*, *22*(5), 1799–1827. Retrieved from http://www.ann-geophys.net/22/1799/2004/ doi: 10.5194/angeo-22-1799-2004

Radioti, A., Grard, J.-C., Grodent, D., Bonfond, B., Krupp, N., & Woch, J. (2008).

Discontinuity in Jupiter's main auroral oval. *J. of Geophys. Res.: Space Physics*, *113*. doi: 10.1029/2007JA012610

Ray, L. C., Achilleos, N. A., Vogt, M. F., & Yates, J. N. (2014). Local time variations in Jupiter's magnetosphere-ionosphere coupling system. *J. of Geophys. Res.: Space Physics*, *119*(6), 4740–4751. doi: 10.1002/2014JA019941

Ray, L. C., & Ergun, R. E. (2012). Auroral Signatures of Ionosphere-Magnetosphere Coupling at Jupiter and Saturn. In A. Keiling, E. Donovan, F. Bagenal, & T. Karlsson (Eds.), *Geophysical monograph series* (Vol. 197, pp. 205–214). American Geophysical Union. Retrieved 2019-03-06, from `http://www.agu.org/books/gm/v197/2011GM001172/2011GM001172.shtml` doi: 10.1029/2011GM001172

Ray, L. C., Ergun, R. E., Delamere, P. A., & Bagenal, F. (2010). Magnetosphere-ionosphere coupling at Jupiter: Effect of field-aligned potentials on angular momentum transport. *Journal of Geophysical Research: Space Physics*, *115*. Retrieved from `http://doi.wiley.com/10.1029/2010JA015423` doi: 10.1029/2010JA015423

Ray, L. C., Ergun, R. E., Delamere, P. A., & Bagenal, F. (2012). Magnetosphere-ionosphere coupling at Jupiter: A parameter space study. *Journal of Geophysical Research: Space Physics*, *117*. Retrieved from `http://doi.wiley.com/10.1029/2011JA016899` doi: 10.1029/2011JA016899

Smith, E. J., Davis, L., Jones, D. E., Coleman, P. J., Colburn, D. S., Dyal, P., ... Frandsen, A. M. A. (1974). The planetary magnetic field and magnetosphere of Jupiter: Pioneer 10. *Journal of Geophysical Research*, *79*(25), 3501–3513. Retrieved from `http://doi.wiley.com/10.1029/JA079i025p03501` doi: 10.1029/JA079i025p03501

Southwood, D. J., & Kivelson, M. G. (2001). A new perspective concerning the influence of the solar wind on the Jovian magnetosphere. *Journal of Geophysical Research: Space Physics*, *106*. Retrieved from `http://doi.wiley.com/10.1029/2000JA000236` doi: 10.1029/2000JA000236

Stallard, T. S., Burrell, A. G., Melin, H., Fletcher, L. N., Miller, S., Moore, L., ... Johnson, R. E. (2018). Identification of Jupiters magnetic equator through H3+ ionospheric emission. *Nature Astronomy*, *2*(10), 773-777. doi: 10.1038/s41550-018-0523-z

Thomas, N., Bagenal, F., Hill, T., & Wilson, J. K. (2004). The Io Neutral Clouds and Plasma Torus. In F. Bagenal, T. Dowling, & W. McKinnon (Eds.), *Jupiter the planet, satellites and magnetosphere* (p. 561 - 591). Cambridge: Cambridge University Press.

Vasyliunas, V. (1983). Plasma Distribution and Flow. In A. Dessler (Ed.), *Physics of the jovian magnetosphere* (p. 395 - 453). Cambridge: Cambridge University Press.

Walker, R. J., & Ogino, T. (2003). A simulation study of currents in the Jovian magnetosphere. *Planetary and Space Science*, *51*(4), 295–307. doi: 10.1016/S0032-0633(03)00018-7

Figure 1.

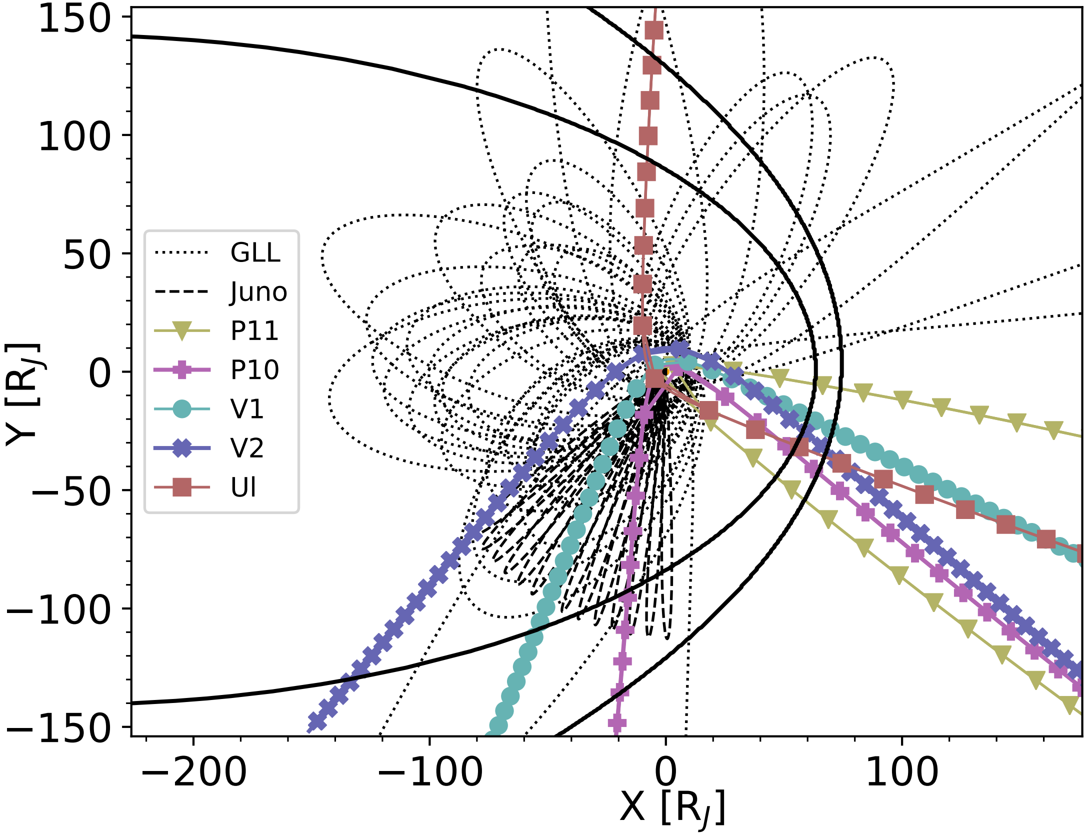

150
100
50
0
−50
−100
−150
Y [R$_J$]
−200
−100
0
100
X [R$_J$]
GLL
Juno
P11
P10
V1
V2
UI

Figure 2.

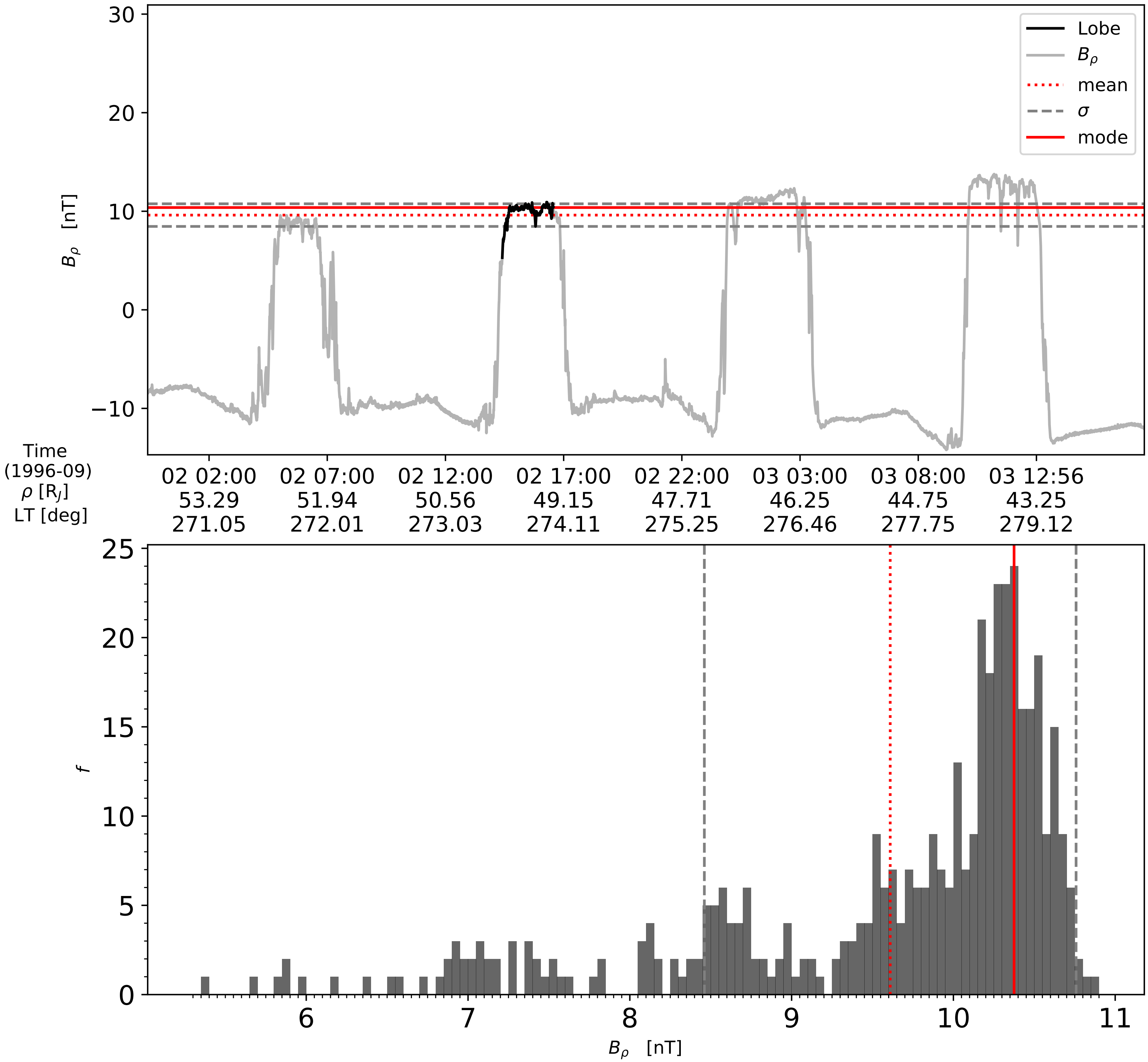

Lobe
B_ρ
mean
σ
mode
B_ρ [nT]
Time (1996-09)
ρ [R$_J$]
LT [deg]
02 02:00 53.29 271.05
02 07:00 51.94 272.01
02 12:00 50.56 273.03
02 17:00 49.15 274.11
02 22:00 47.71 275.25
03 03:00 46.25 276.46
03 08:00 44.75 277.75
03 12:56 43.25 279.12
f
B_ρ [nT]

Figure 3.

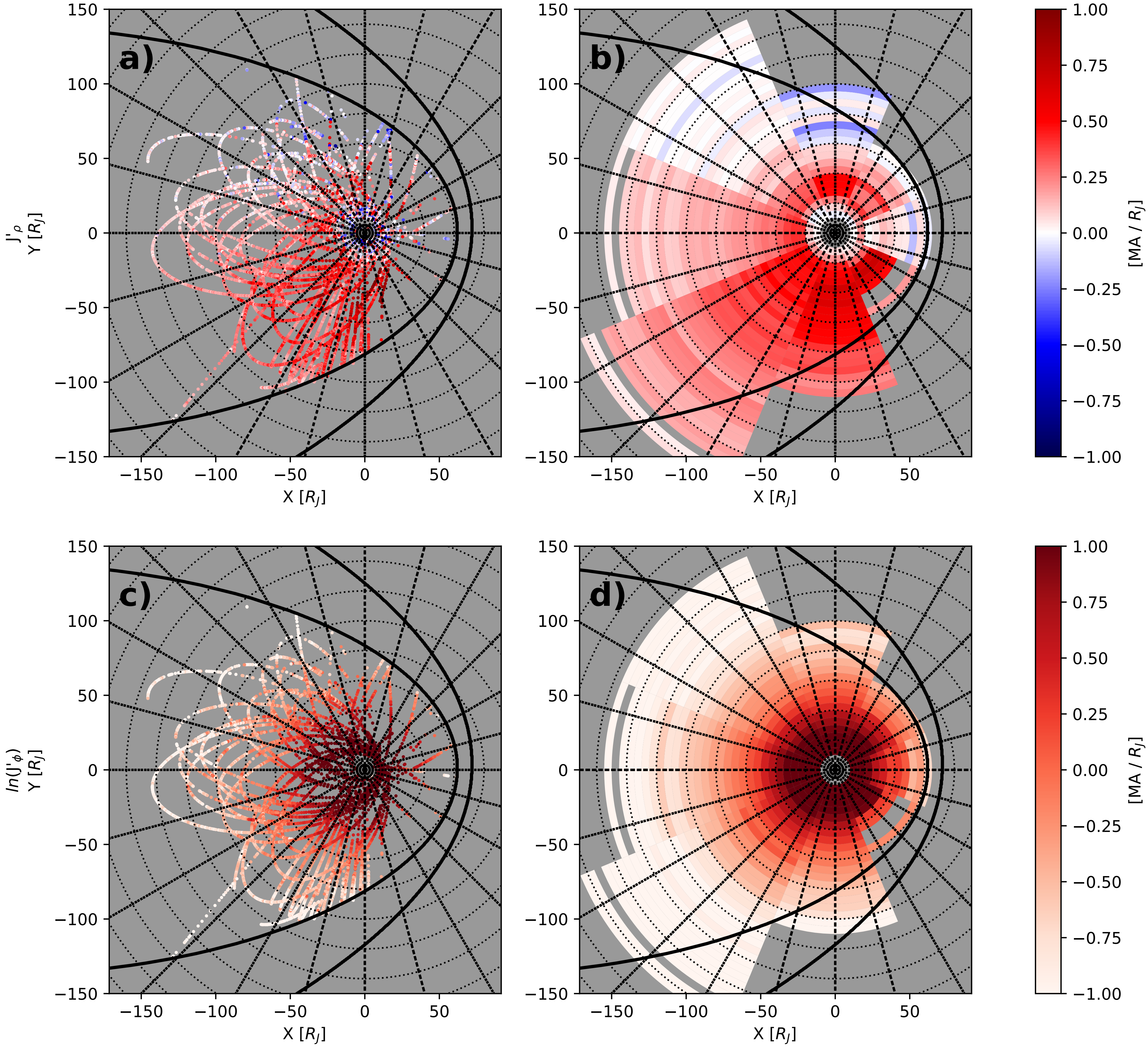
a)
b)
c)
d)
J'$_\rho$
Y [R_J]
ln(J'$_\phi$)
Y [R_J]
X [R_J]
[MA / R_J]
150
100
50
0
−50
−100
−150
−150
−100
−50
0
50
1.00
0.75
0.50
0.25
0.00
−0.25
−0.50
−0.75
−1.00

Figure 4.

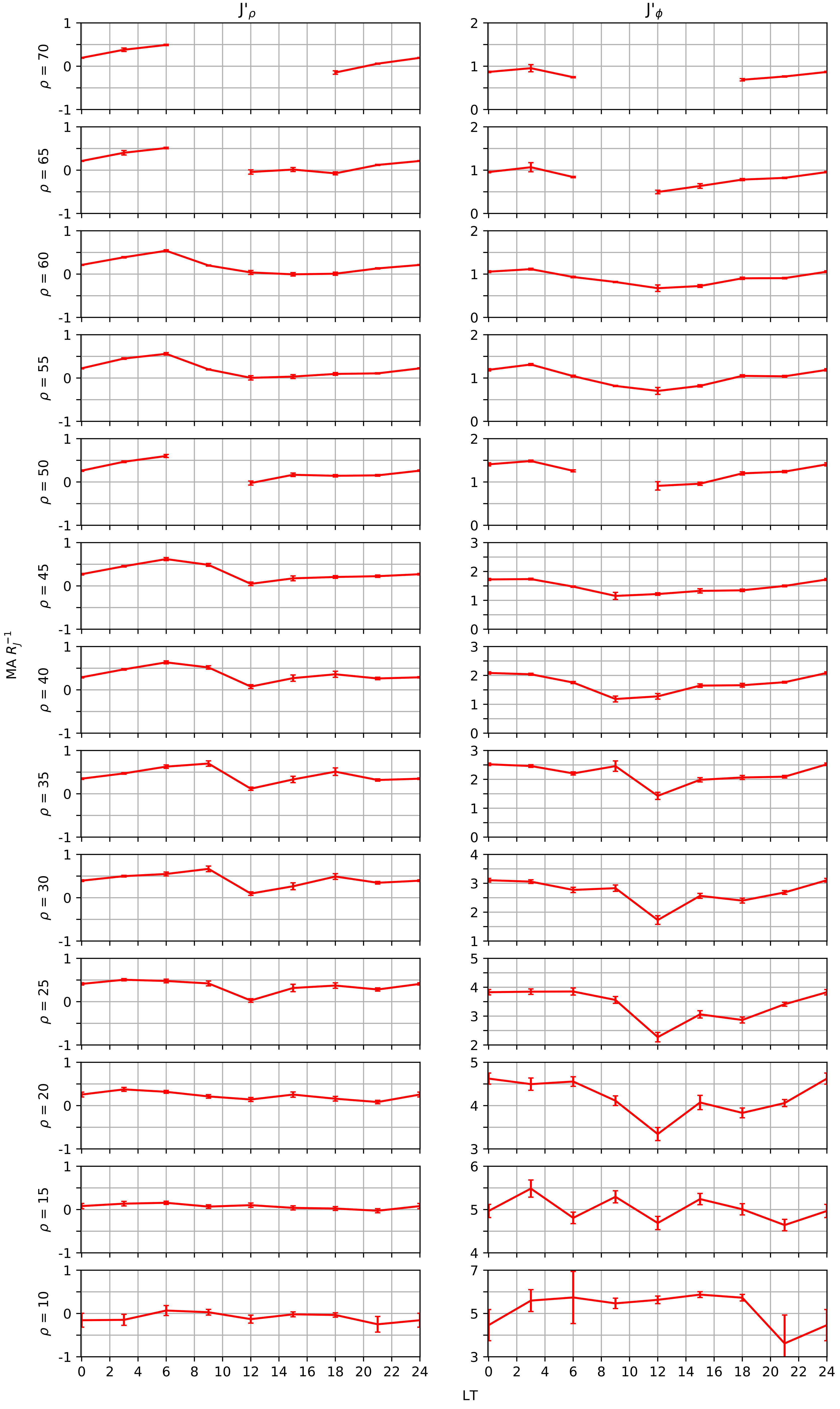

J'$_\rho$
J'$_\phi$
ρ = 70
ρ = 65
ρ = 60
ρ = 55
ρ = 50
ρ = 45
ρ = 40
ρ = 35
ρ = 30
ρ = 25
ρ = 20
ρ = 15
ρ = 10
MA R_J^{-1}
LT

Figure 5.

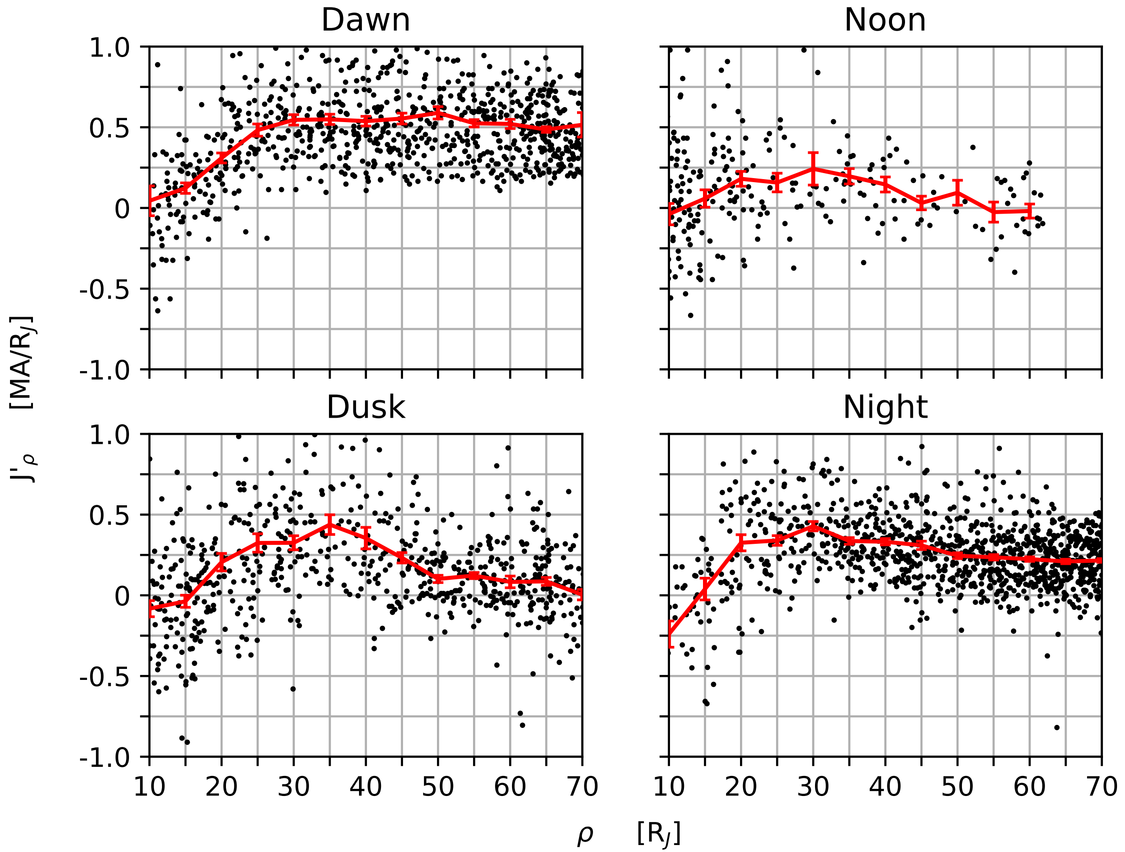

Dawn
Noon
Dusk
Night
1.0
0.5
0
-0.5
-1.0
10
20
30
40
50
60
70
J'$_\rho$ [MA/R$_J$]
ρ [R$_J$]

Figure 6.

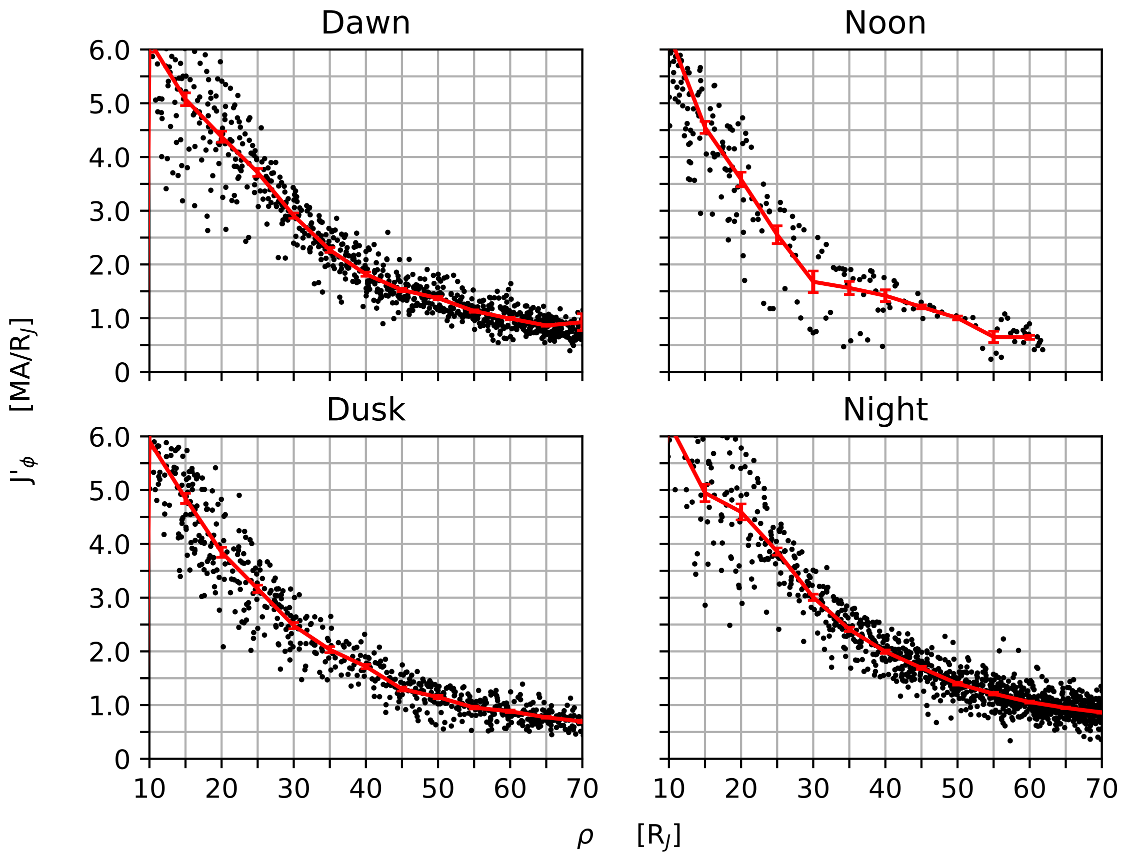

Dawn
Noon
Dusk
Night
J'$_\phi$ [MA/R$_J$]
ρ [R$_J$]
6.0
5.0
4.0
3.0
2.0
1.0
0
10
20
30
40
50
60
70

Figure 7.

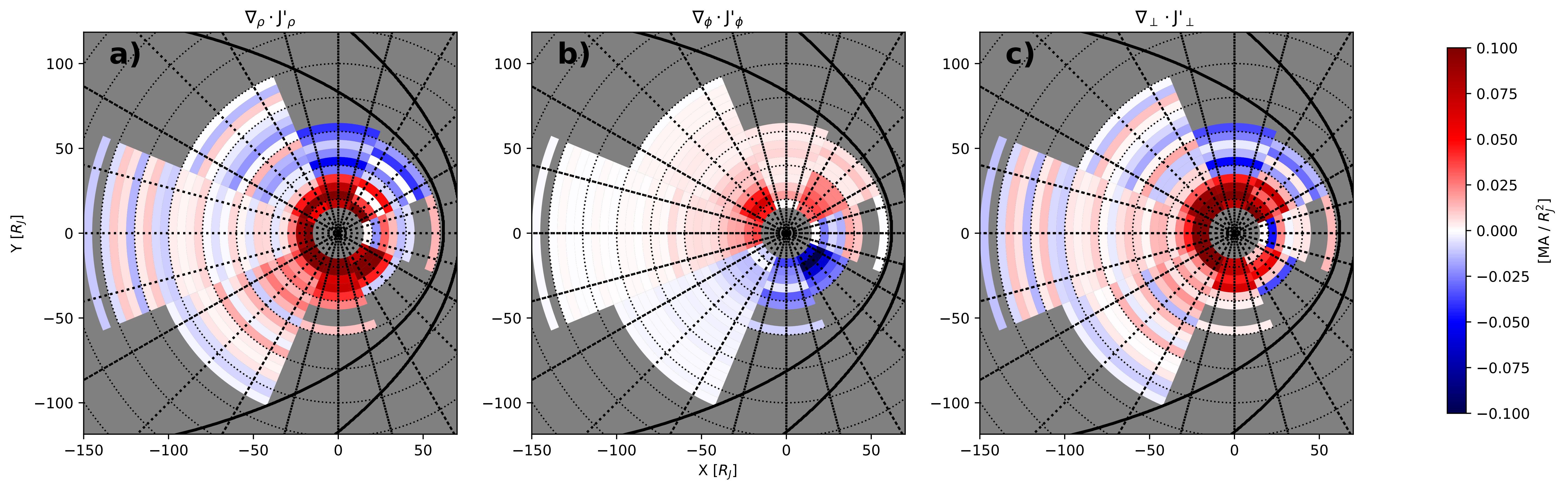

$\nabla_\rho \cdot J'_\rho$
$\nabla_\phi \cdot J'_\phi$
$\nabla_\perp \cdot J'_\perp$
a)
b)
c)
Y $[R_J]$
X $[R_J]$
$[MA / R_J^2]$
0.100
0.075
0.050
0.025
0.000
−0.025
−0.050
−0.075
−0.100
100
50
0
−50
−100
−150

Figure 8.

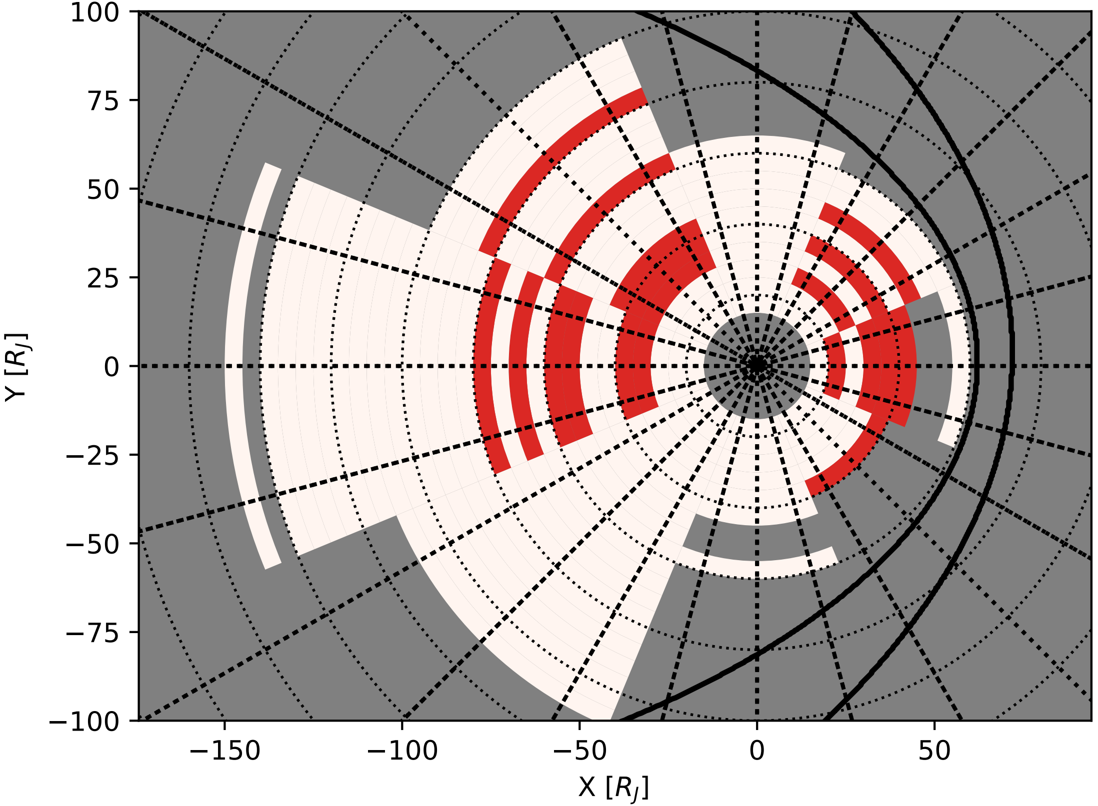

100
75
50
25
0
−25
−50
−75
−100
Y [R_J]
−150
−100
−50
0
50
X [R_J]